Local Electric Fields in Dielectric and Semiconductors: Part II

Dmitry E. Milovzorov

Abstract

Local electric fields appeared in dielectric and semiconductors due to the destruction of symmetry, creating the vacancies, point defects, and chemical impurities in material. By increasing external electric field value, numerous structural changes will be generated. Point defects in silicon films were characterized by using electron-paramagnetic resonance spectroscopy and laser picosecond spectroscopy. EPR spectroscopy provides the detailed microscopic information about the point defects in silicon films, which have unpaired electrons. The switching effect for A or $(VO)^-$ defects was observed by applied bias voltage for nanocrystalline silicon films. The intensities of EPR signal change according to the switching of position of oxygen incorporated in silicon (111) from one pair of silicon atom to another pair of silicon atoms. In this case, the interaction between p_x orbital is changed to p_z orbital. The proposed mechanism of states' switching for the vacancy $(VO)^-$ is based on a model of coupled dangling bonds (DBs) of silicon atoms and interaction between atomic orbitals. The crystal phase destruction in nanocrystalline silicon film by applying external electric field was investigated by Raman spectroscopy. The possible mechanism of phase creation was proposed.

Keywords: local field, point defect, dangling bonds, Raman spectroscopy, nanocrystals, second-harmonic generation, silicon films

1. Introduction

Local electric fields appeared in dielectric and semiconductors due to the destruction of symmetry, creating the vacancies, point defects, and chemical impurities in material. By increasing external electric field value, numerous structural changes will be generated. Some of them will produce such great local fields that will destroy all material or change its physical properties. Studying the nature of local electric fields will open new tendencies in electronic

device producing, from one side, and help to change materials' properties according to our needs, from another side. The quantum size effect for nanocrystalline silicon films with broad size distribution was observed by PL and SHG spectral measurements. The optical properties of films are likely to depend on the size distribution of nanocrystals, along with an effect of hydrogen termination on the surface of nanocrystals. The studying of physical properties of such nanoscale objects as nanocrystals, point defects and chemical bonds is very important for understanding the appearance of local fields in silicon films, as it is necessary to investigate them and to detect the physical phenomena which appear due to the local fields. For small particles such as electron, the wave features play a significant role because the de Broglie wave length is given by $\lambda = \frac{h}{p}$; where p is impulse and h is Planck constant. For electron rotating around nucleus of atom with circulation rate 3.54×10^6 m/s, $\lambda_{DB} = 2.5$ Å. For oxygen atom at room temperature and the rate of motion 250 m/s, the de Broglie wavelength is $\lambda_{DB} = 2.0$ Å. The probability of occupancy of each energy state is defined by wave function as a solution of the Schrodinger equation $H\psi = i\hbar\frac{\partial\psi}{\partial t}$; where H is full energy of system named as Hamiltonian. For example, for the quantum well with the size L = 100 Å, the solution of this equation is satisfied to a discrete energy according to the following expression $E_n = \frac{\pi^2\hbar^2}{2mL^2}n^2$, where numerical data are 3.37 meV for n = 1, 13.48 meV for n = 2, 30.33 meV for n = 3, and 53.92 meV for n = 4.

2. Quantum objects in silicon films

The probability to find the particle in each state can be calculated as $\rho_{nn} = \left|\psi_n(x)\right|^2$. Hamiltonian of system can be written in following form: $H = \sum\limits_{i=1}^{N} H_i + \sum\limits_{i=1}^{N}\sum\limits_{j=1}^{N} V_{ij}$, where H_i is diagonal matrix element and V_{ij} is an interaction energy or non-diagonal matrix elements. For example, the quantum properties of interaction between the elements are explained by using resonance integrals ($H_{ab} = \int \psi_a H \psi_b d\zeta$), and overlap integrals (e.g., for two 3pSi-3pSi orbitals that are located on different Si atoms $\delta = \int\limits_{0}^{2\pi}\int\limits_{0}^{2\pi}\int\limits_{0}^{\infty} \psi_{3pxSi}\psi_{3pxSi} r^2 \sin\varphi \cos\varphi \sin\varphi dr d\varphi d\varphi$) which can be calculated for a small distances: 0.675 for interaction of 3pSi-3pSi orbital and X = 2.35 Å, 0.837 for the same orbital and distance 2.21 Å and 0.0684 for X = 3.65 Å, 0.0484 for X = 3.83 Å; and by X = 9 Å it is 5.3×10^{-7}. For orbital interaction of $3p_xSi$-$2p_xO$, for X = 2.21 Å, the overlap integral equals to $2.8\ 10^{-6}$, for X = 2.35 Å it is 1.2×10^{-6}, for X = 3.65 Å it is $3.1\ 10^{-10}$, for X = 3.83 Å it is 9.55×10^{-11} because the quantum phenomena can be surely observed on such scale as it is seen.

2.1. Nanocrystals in silicon films

The combination of laser picosecond spectroscopy with Raman scattering measurements is perspective for nondestructive analysis of composite thin films and silicon surface with complex relief. The method of laser picosecond spectroscopy is a powerful tool for surface analysis

with high sensitivity. The pump-probe scheme is similar to the interferometric schemes with great possibility to measure the refractive index changes. For composite thin film measurements, such as poly-Si or porous silicon, the local factor field plays a great role because the crystalline volume fraction (or porosity) and dielectric functions' values of film's components are important. Also, due to the great amount of scattering centers (e.g., nanocrystallites or microcrystallites spatial distribution in film according to Gaussian distribution), the role of photo-acoustic distortion is negligible. However, the non-equilibrium perturbation of career density and its decay due to the diffusion or recombination (in case of great porosity or small value of ρ) are detected surely by using picosecond technique. In addition, it is necessary to note that the electron relaxation from surface and defect states can be reflected by optical response evolution, too. Also, by carrying these measurements, it is important to know the surface morphology. For elimination of the surface scattering background the correlation function value was measured.

2.1.1. Nanocrystal detection by Raman spectroscopy

The Raman spectra for poly-Si films consist of a narrow line near 520 cm^{-1} arising from a crystalline phase and a broad line around 480 cm^{-1} from an amorphous phase. The ρ value was estimated from the ratio of the Raman integrated intensity for the crystalline component to the total intensity, using the ratio of the integrated Raman cross-section for the crystalline phase to that of an amorphous phase. The penetration depth of the incident Ar-ion laser radiation ($\lambda = 488$ nm) into silicon is within about 0.3 μm.

The crystalline volume fraction was estimated using Raman scattering measurements from the ratio [1]: $\rho = \frac{I_c}{I_c + I_a}$, where I_c is the Raman integrated intensity for the crystalline component (sharp peak at 520 cm^{-1}) and Ia is for amorphous phase (smooth peak at 480 cm^{-1}). The random silicon network is Gauss distributed in their bond lengths with various deviations, and phonon wave numbers is spread. The regular bonding network has the Lorentz shape of its spectral line. Our possible interpretation of a-Si Raman spectra decomposition is to recognize the defects and impurities which cause the changes in electrical properties of films. We guess that the a-Si film with high density of defects such as silicon vacancies causes the spectral peak around 465 cm^{-1}, but after annealing there is a spectral shift in wave number 465 cm^{-1}➔475 cm^{-1}. By hydrogen dilution of gas mixture by PECVD of a-Si the Raman peak position is changed from 475 cm^{-1} to the 480 cm^{-1} [2].

It was assumed that this change is because the bond angle variation value decreases by the starting crystallization process in a-Si film. We assume that the Raman data of hydrogenized amorphous silicon film resulting in the spectral peak around 445–447 cm^{-1} corresponds the LO mode but it is 480 cm^{-1} for TO mode. For the higher structural relaxed silicon thin film, by high level of hydrogen dilution, the TO mode reflects in 490 cm^{-1} value of peak position. The spectral peak width changes from the value of 40 cm^{-1} for a-Si to the 70 cm^{-1} for a-Si:H.

Figure 1 shows the various types of decompositions of Raman spectrum for microcrystalline silicon film with thickness around 100 nm. This film was deposited at 380°C. By using this procedure we use 3, 4, and even 9 peak approximations. The figure illustrates the three-peak
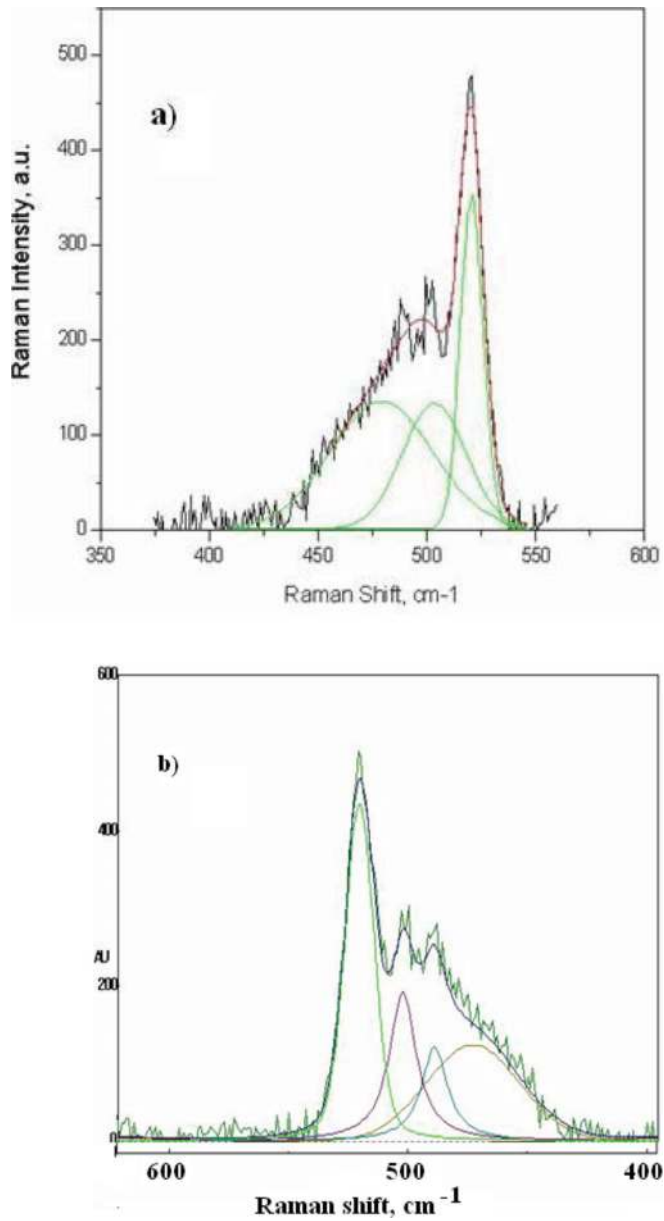
Figure 1. Raman spectra deconvolution by using (a) 3 peaks approximation: c-Si, for 520 cm^{-1}; a-Si for 480 cm^{-1} and intermediate or nanocrystalline for 500–510 cm^{-1}; (b) 4 peaks approximation: for c-Si (520 cm^{-1}); a-Si (480 cm^{-1}); nanocrystalline (500–510 cm^{-1}) and hydrogenated a-Si:H for 490 cm^{-1}; approximation for different silicon networks for TO phonon modes: c-Si, nc-Si, a-Si, a-Si:H, a-Si high hydrogenated, a-Si with different defects; and for LO phonon modes in a-Si; a-Si:H.

decomposition with c-Si-related spectral line around 520 cm^{-1}, nanocrystalline or intermediate spectral line in the range 500–510 cm^{-1} and for amorphous silicon it is 480 cm^{-1}. The next figure, **Figure 1b**, shows the Raman data with noise signal for comparison, and fourth spectral component (~490 cm^{-1}) is related to hydrogenated amorphous silicon network. The estimation of crystalline volume fraction was 27%. The hydrogen terminates all the dangling bonds (DBs). The spectral characteristics of amorphous-related peaks are changed by the hydrogen saturation of dangling bonds.

2.1.2. Time-resolved picoseconds laser spectroscopy of silicon nanocrystalline films

A mode-locked YAG:Nd^{3+} laser radiation with wavelength 532 nm was used as an optical pump of media, but the second-harmonic radiation (λ = 1064 nm) was used for probing the sample's **Figure 2**. The correlation between the reflected signal intensity and probe laser beam for a-Si and p-Si films surface is given. The pulse duration was 120 ps. The pulse repetition rate was 100 MHz and frequency of Q-switched modulation of second-harmonic radiation was 6.2 MHz.

The correlation function of reflected signal intensity of probe laser beam was detected by means of pump-probe laser scheme $G(t) = < I(t)I(t+\tau) > = \frac{1}{T}\int_0^T I(t)I(t+\tau)dt$; where G (t) is the averaged correlation function and T is the time of detection. It is seen that $G(t) \sim exp.$ $(-\Delta\omega t)$; $\Delta\omega$ is a width of level that is equals 8 µeV for porous silicon, and 16 µeV for a-Si:H. Figure illustrates the time evolution of correlation function for the amorphous silicon (a-Si)
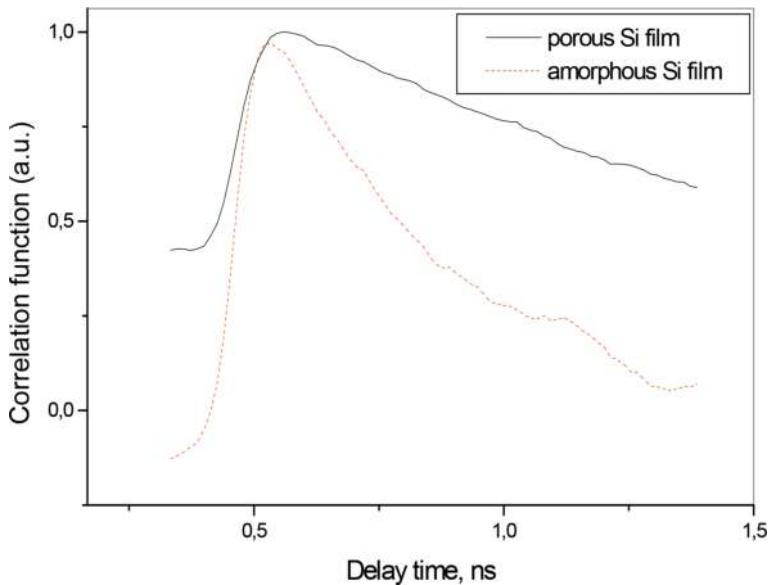

Figure 2. Evolution of correlation function for the amorphous silicon and porous silicon.

surface and porous silicon (por-Si) sample prepared by the value of current 5 mA/cm^2 in hydrofluoric acid (HF)/ethanol solution by the ratio 1:1. It is seen that the time decay of relative reflected intensity of signal for por-Si is slightly less due to the prepared nanostructured surface compared with a-Si. It is supposed that the time evolution corresponds to the surface electronic band structure. Also, we proposed the formula for estimation of recombination rate from the Fermi golden rule:

$$\tau^{-1} = \frac{16\pi^2}{3} n \frac{e^2}{h^2 m^2 c^3} E |< i|p|j >|^2 \tag{1}$$

where E is transition energy and < i| and |j > are the initial and final states of electron transition. The time evolution reflects the superposition of ensemble of different kinds of transitions such as band-to-band transition, transition through the surface or defect states. The width of the energy level depends on the chemical bond structure of silicon surface. The most important fact is appearance of quantum beats, which reflect the optical response from two-neighbor level. We suppose that the different fractions of oxygen incorporation in silicon film cause the production of neighbor levels inside the band gap with the spectral width: $\Delta = \frac{20\varepsilon_x h^3}{m^2 e^2} N$ a-Si reflects the presence of complex SiO configuration. The figure shows the correlation function as a function of delay time for oxidized Si (111) surface and poly-Si silicon film with <δ> = 9.7 nm. It is expected that the oxide defect levels and surface state level (for Si (111) surface) are responsible for the observed oscillation during the exponential decay of electron density. We suggest that such oscillations are the same as quantum beats of levels of occupation by the laser time-resolved spectroscopy of molecular levels with the period of ΔT. Also, it is seen that exponential decrement for poly-Si film is weaker than the other. It is assumed that the correspondence between the values of decrement and width of oxygen-related levels in the band gap of silicon is proved and the magnitude of correlation function oscillations illustrates oxide amount on the surface. Also, our assumption has strong evidence from the FTIR data for aged poly-Si films.

Intervalley scattering rate is given by [3]

$$\frac{1}{\tau_{\text{intervalley}}} \propto N_q \left(E_k + E_p\right)^{1/2} + \left(N_q + 1\right)\left(E_q - E_p\right)^{1/2} U\left(E_k - E_p\right); \tag{2}$$

where E_p is the phonon energy and U is the step function. For TA or LA phonon modes (with energies 10 meV) we can estimate the intervalley rate at around 2.5 10^{12} Hz. Figure illustrates quantum beats observed in correlation function's evolution for oxidized surfaces: Si (111) surface and silicon film with <δ> = 9.7 nm. The period of quantum beats is estimated as ΔT=h/Δ. Width for level is Δω = 6 μeV for Si(111) surface but gap is Δ = 7.2 μeV, and Δω = 7.2 μeV and Δ = 12 μeV for silicon film with <δ> = 9.7 nm. It is seen in **Figure 3** that correlation function depends on the time according to exponential law with harmonic modulation of intensity because of quantum interference of levels $G(t) \sim exp.(-\Delta\omega t)(1 + Ccos(\Delta t))$; Δω is a width of level and Δ is an energy gap between the two closed levels (see **Figure 4b**).

Dipole moment can be written in form [4]

$$d = \frac{er}{2} \frac{\left(\phi_2 - \phi_1\right)^2}{\left(\phi_2 - \phi_1\right)^2 + 4J^2(r)}[n_2(t) - n_1(t)]; \qquad (3)$$

where $n_2(t)$ and $n_1(t)$ are levels populations, J is resonance integral, and φ_1 and φ_2 are energies of electrons. Reflected intensity harmonic oscillations can be explained by using time-dependent dipole moment of coupled atoms of Si-Si bonding.

In conclusion, the new method of laser spectroscopy for testing nanocrystal silicon structures and measurements of band gap energy and energy position of defect levels inside the band gap is proposed. Also, the competition between the electron diffusion and recombination processes in poly-Si films by the transmitted probe-pump laser scheme is analyzed. It is clear that tunneling process between the silicon nanocrystals through the thin oxidized layer plays a great role and it is possible to design a new electronic device.

2.2. Point defects in silicon

For several decades, a-Si:H films are intensively studied by different spectroscopic and microscopic methods. Most of the a-Si films contain some amount of nanocrystals. This is because
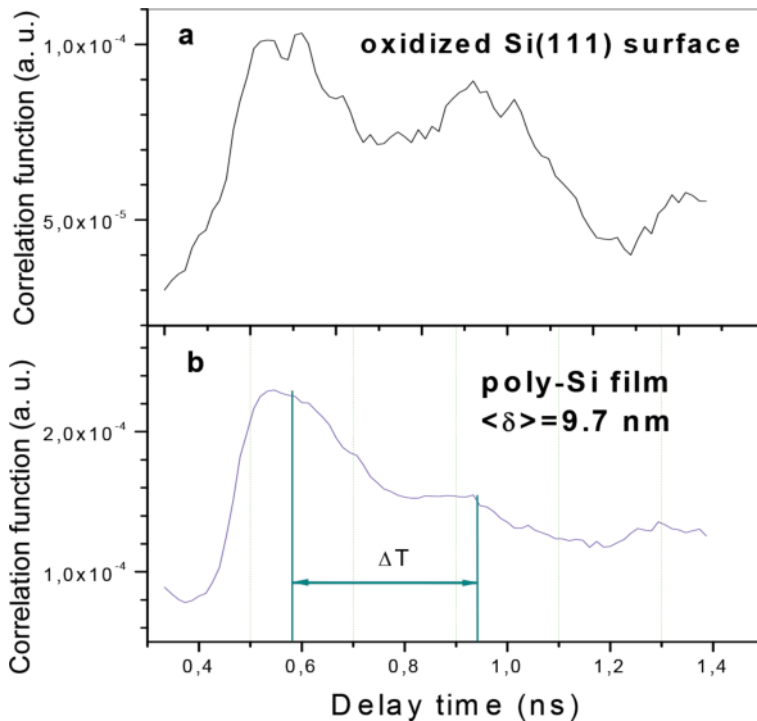

Figure 3. Quantum beats observed in correlation function's evolution for oxidized surfaces: Si (111) surface (a) and poly-Si film with <δ> = 9.7 nm (b). The period of quantum beats is ΔT=h/Δ.
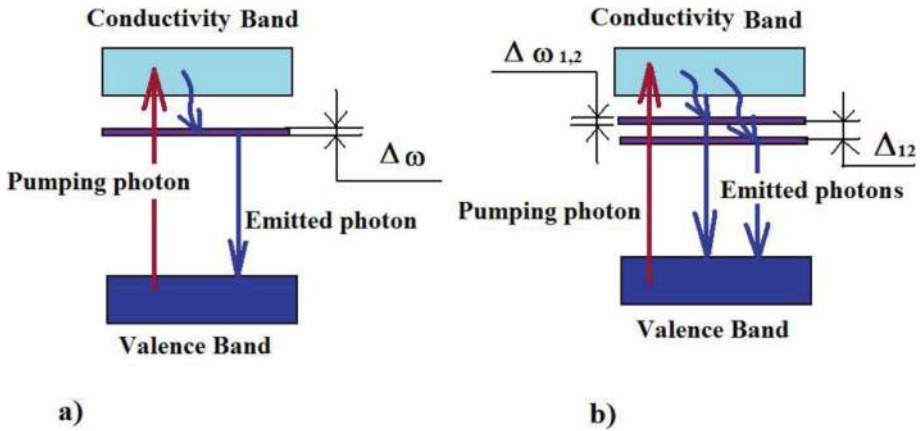
Figure 4. Energy diagrams and scheme of laser pump and light emission. The emission of light is realized by the carriers recombination through the one defect level (a) with spectral width Δω, and two defect levels which are located closed to each other (b) with energetic gap Δ_{12}.

the PECVD method to prepare nc-Si films and a-Si films is the same but differs only in deposition conditions such as substrate temperature, gas mixture, working pressure, and RF power. **Figure 5** illustrates the CVD-prepared a-Si film with gas silane by 1 sccm flow rate. The RF power was 20 W and temperature of substrate was 25°C. It is clear that the sharp peaks relate to the various fractions of silane dissociation: $(SiH)_x$; $(SiH_2)_x$; $(SiH_3)_x$; $(SiH_4)_x$. It is

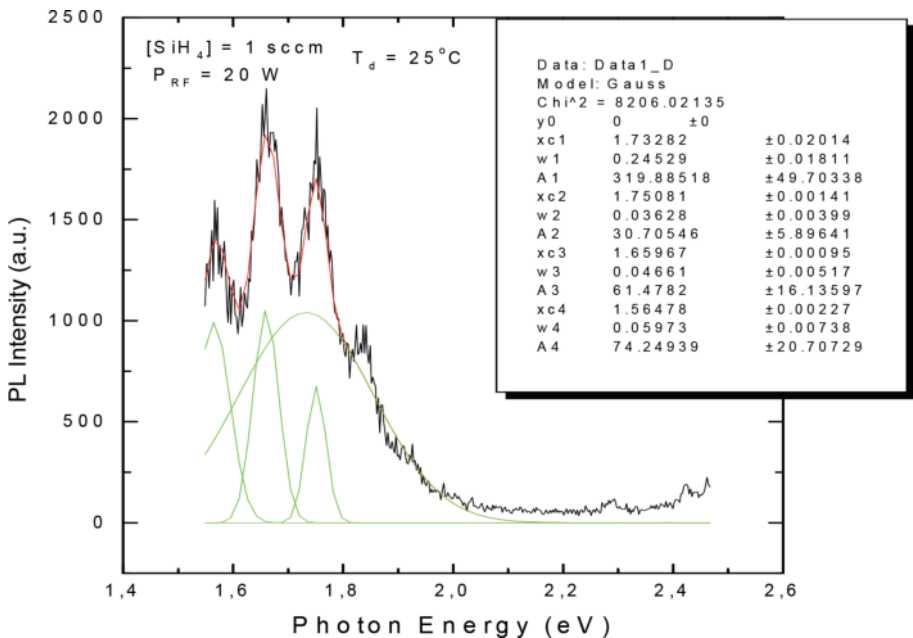| Data: Data1_D		
Model: Gauss		
Chi^2 = 8206.02135		
y0	0	±0
xc1	1.73282	±0.02014
w1	0.24529	±0.01811
A1	319.88518	±49.70338
xc2	1.75081	±0.00141
w2	0.03628	±0.00399
A2	30.70546	±5.89641
xc3	1.65967	±0.00095
w3	0.04661	±0.00517
A3	61.4782	±16.13597
xc4	1.56478	±0.00227
w4	0.05973	±0.00738
A4	74.24939	±20.70729

Figure 5. Photoluminescence spectrum of a-Si film.

supposed that their responses are around spectral lines: 1.56, 1.65, 1.73, and 1.83 eV. Also, the broad spectral peak around 1.75 eV is related to the tiniest nanocrystals in a-Si film.

EPR spectroscopy provides the detailed microscopic information about the point defects in silicon films, which have unpaired electrons. It is seen in **Figure 6**, that there is a dangling bond signal on EPR spectrum. Therefore, the a-Si films contain dangling bond defects and are disordered due to the hydrogen termination of dangling bonds. The surface diffusion and desorption processes by growth are low at low temperatures of deposition.

2.2.1. Dangling bonds

For detail explanation of dangling bond (DB) defects several kinds of models were proposed such as defect-pool model of Powell and Dean [5]. The main principle of this model is the following. There is equilibrium between the quantity of dangling bonds and weak bonds. The chemical reactions that cause the appearance of dangling bonds are the following: WB $\Leftrightarrow$ (2DB); SiH + WB $\Leftrightarrow$ (DB + SiH) + DB; 2SiH + WB $\Leftrightarrow$ (Si-H-H-Si) + 2DB. Thin film deposition at low temperatures of substrates results in the appearance of dangling bonds defects that can be terminated by hydrogen. The process of nucleation of crystal grains required the minimum quantity of silicon atoms.

These paramagnetic centers appear when there is an unpaired electron of the dangling bond of silicon atom that bonded with three silicon atoms (see **Figure 7**).

For coupled dangling bonds of silicon atoms on the surface (111) there is an interaction between atomic orbitals (as it is seen in **Figure 8**). The degeneracy of the level according to rules for wave functions of one silicon atom with free atom $3pSi_x$ orbital and the other silicon atom with one $3pSi_z$ orbital is $\Psi^+ = \Psi_{3pSix} + \Psi_{3pSiz}$; $\Psi^- = \Psi_{3pSix} - \Psi_{3pSiz}$. Coupling two dangling bonds are transformed into A
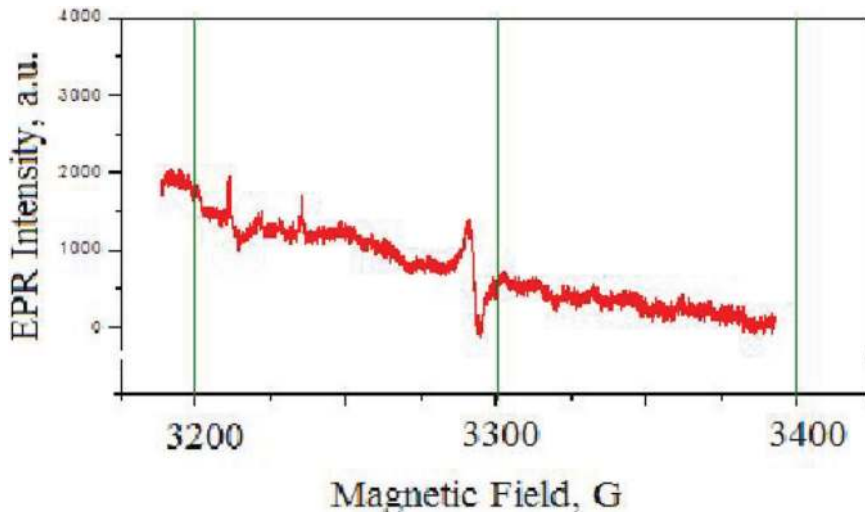

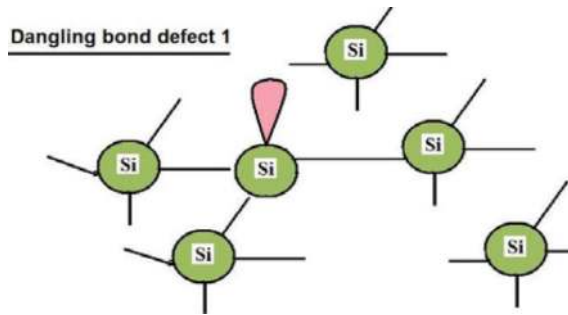**Figure 6.** EPR data for a-Si film with dangling bonds defects.

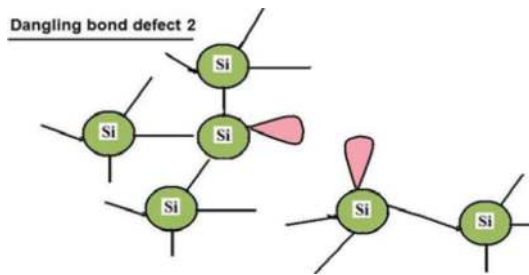**Figure 7.** Dangling bond on the silicon (111) surface.

Figure 8. Dangling bonds defect in silicon crystalline (111) film.

defect with coupling bonds by the following way according to Elsner's theorem of matrix perturbation theory: $\begin{pmatrix} H_{11} & \varepsilon \\ \varepsilon & H_{22} \end{pmatrix} \rightarrow \begin{pmatrix} \hat{H}_{11} & 0 \\ 0 & \hat{H}_{22} \end{pmatrix}$, where $\lambda'_1 \leq \left(\|H_{11}\| + \|\hat{H}_{11}\| \right)^{-1/2} \|\varepsilon\|^{1/2}$;

$\lambda'_2 \leq \left(\|H_{22}\| + \|\hat{H}_{22}\| \right)^{-1/2} \|\varepsilon\|^{1/2}$; are the eigenvalues for $(\hat{H}_{11}\, 0\, 0\, \hat{H}_{22})$ system. Spectral characteristics of eigenvalues $\hat{\lambda}'_1, \hat{\lambda}'_2$ become broader by each bonding transformation or switching because there is a great difficulty to define the final state.

2.2.2. Vacancies and oxygen incorporated in silicon (111)

At first time the term A defect (or center) in silicon was used by Watkins and Corbett in 1961 [6]. They studied the irradiated by 1.5 MeV electron beam silicon with current density 2.5 μa/cm². The role of oxygen in A center creation is significant due to its definite bonding with silicon atoms. Spin resonance is caused by unpaired electrons which is trapped by splitting of the atomic orbital of pair-coupled silicon atoms. The figure illustrates the appearance of A defect paramagnetic centers in inter-grain area of nanocrystalline silicon films experimentally detected by means of the EPR spectrometer technique.

Figures 9 and **10** show the switching effect for A centers by applied bias voltage for fluorinated nanocrystalline silicon films. The intensities of EPR signal change according to the switching of

position of oxygen incorporated in silicon (111) from one pair of silicon atom to another pair of silicon atoms. In this case the interaction between p_x orbital is changed to p_z orbital. The frequencies of spectral component of EPR related to A defect on Si (100) surface disappeared by the annealing procedure because of surface thermo-diffusion.

Figure 11 presents the various pictures of potential energy for oxygen atom bonded with couple Si atoms as a function of a distance by classical approach. It is clear that the distances that characterize the motion of oxygen atom are compared with its de Broglie wave length (2–4 Å) because there is a possibility to use quantum mechanical treatment of moving oxygen atom caused by the electric field from one silicon atom pair to another. **Figure 12** shows the scheme of Si-O-Si bridge with coupled Si-Si atoms as the quantum oscillator with eigenvalues of energy of the oxygen atom.

The oxygen atoms and dimers are incorporated in the silicon grain boundary and have weak covalent bonds with silicon. But the activation energy for molecular diffusion is low, 0.3 eV, in contrast with the activation energy value for atomic diffusion (1.3 eV). The energy of Si-O-Si bridge interaction can be written in form of Morse function
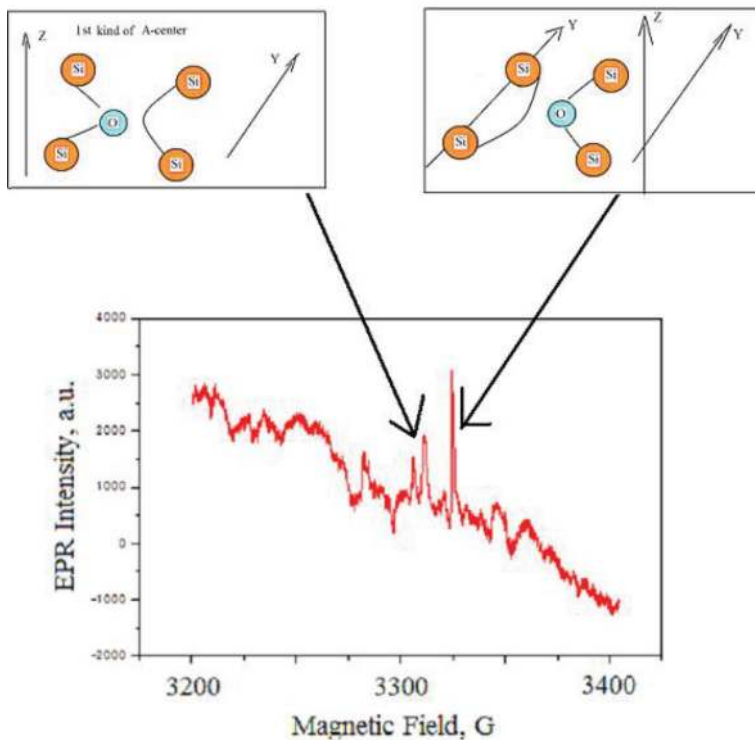

Figure 9. A defect paramagnetic center in inter-grains area of nanocrystalline silicon films detected by EPR spectrometer (Bruker Comp.).
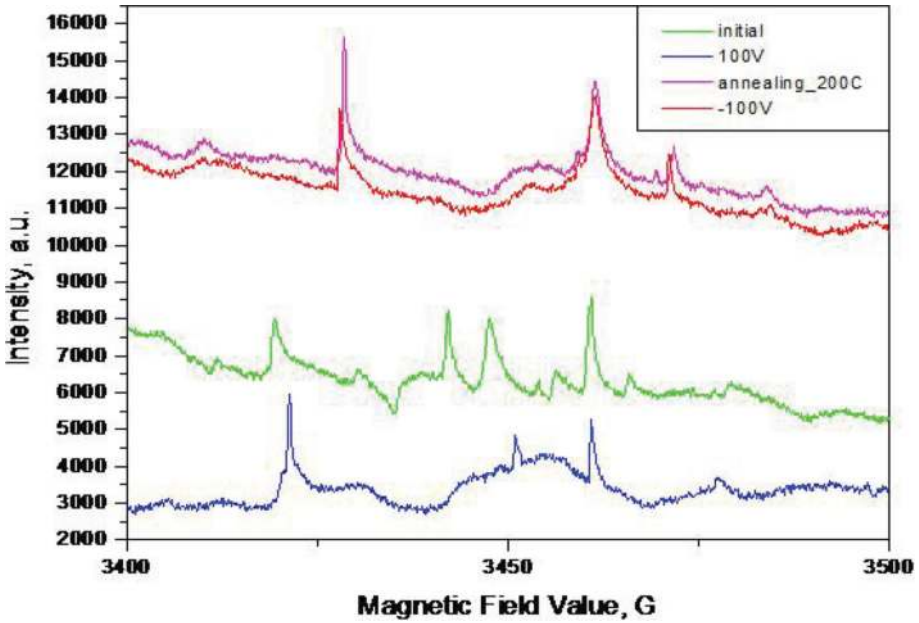
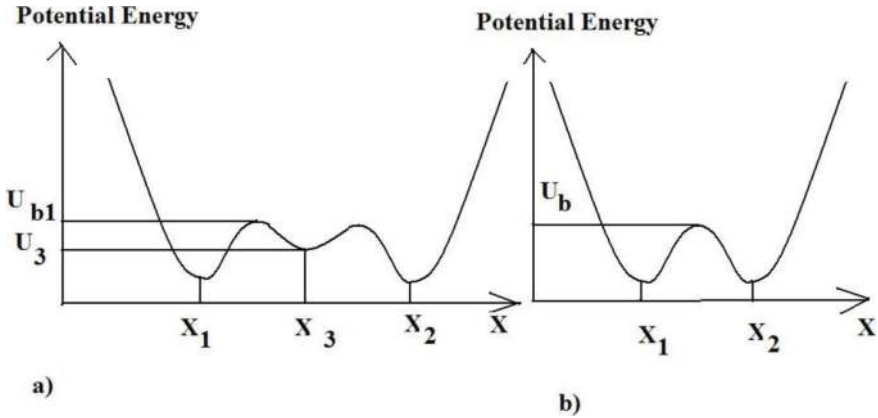**Figure 10.** EPR data for fluorinated nanocrystalline silicon film by applied bias voltage and annealing.

Figure 11. Potential energy of oxygen atom bonded with couple Si atoms.

$$U = U_0\left(1 - \exp(-\alpha(x - d))\right)^2 + U_0\left(1 - \exp(-\alpha(x + d))\right)^2 \qquad (4)$$

where U_0 is the energy of Si-O (4.5 eV) and α is coefficient. The oxygen atom in A center oscillates between two points of stable positions. Transition of probability for oxygen atom through the potential barrier by applied external electrical field $U(r) = U_0 - Er$ is given by
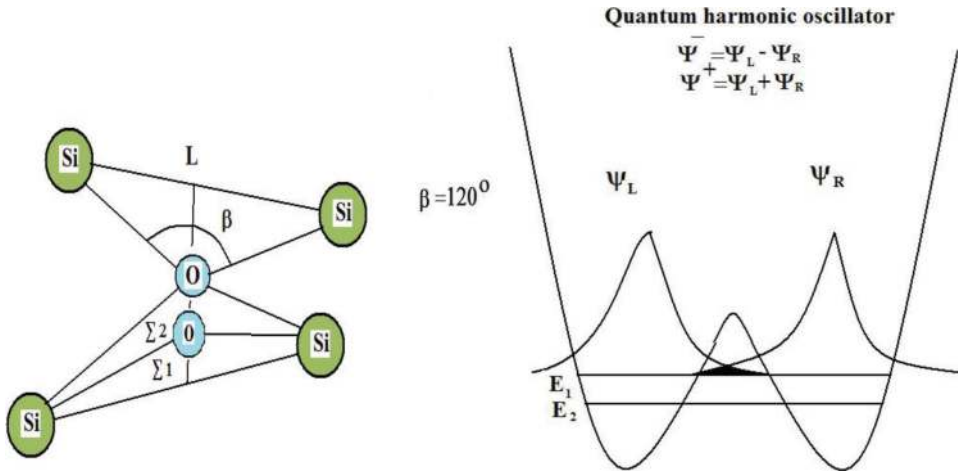
Quantum harmonic oscillator

$$\overline{\Psi} = \Psi_L - \Psi_R$$
$$\Psi^+ = \Psi_L + \Psi_R$$

Figure 12. Scheme of Si-O-Si bridge with coupled Si-Si atoms.

$$T = v\exp\left(-\frac{2}{\hbar}\right)\int_{r_1}^{r_2} dr\sqrt{2M(U(r) - E_l)} \tag{5}$$

where v is a frequency of oscillations of oxygen atom. Wave function of the oxygen atom is the following

$$\Psi = a_1\left|\phi_1 > \exp\left(-i\frac{E_1}{\hbar}t\right)\exp(-\Gamma_1 t) + a_2\right|\phi_2 > \exp\left(-i\frac{E_2}{\hbar}t\right)\exp(-\Gamma_2 t);$$

where φ_1 and φ_2 are the wave functions of pure states 1 and 2 and Γ_1 and Γ_2 are the widths of the levels, respectively. We assume that all the Γ values are approximately equal to each other. Raman scattering data help to determine the dipole Si-Si orientation along the laser E field ax of incident radiation on the silicon surface by applied electric field switching of O atom spatial position. Applied electric field causes the tunnel of oxygen atom from one pair of coupled silicon atoms to another with perpendicular axis of dipole orientation. The annealing procedure can assist to restore spectral characteristics related to the primary-ordered atomic position due to the minimums in potential energy diagrams.

2.2.3. Physical model of vacancy switching by applied electric field

The role of applied electric field in order–disorder transition can be surely understood by using several mechanisms of electric dipole creation as it is seen in **Figure 10**. The first mechanism is the changing length of silicon-oxygen Si-O bond or silicon fluorine (Si-F) bonding and atomic transfer of oxygen inside the vacancy defect which causes the reorientation of VO or VF defects. Such bonds are strongest in silicon film because of high-electron affinity values for O and F atoms. The dipoles Si-O and Si-F have the great value in their polarized charges because the

interaction between them and electromagnetic field is sufficient, and it results in their efficient reorientations because the dipole in external field changes its orientation to compensate it.

The second mechanism of order–disorder transition in the silicon film was initially proposed by Watkins and Corbett [7], which is devoted to hydrogen atom reorientation around the vacancy by the temperature above 200°C as the possible EPR data explanation. For nanostructured silicon thin film that contains a great amount of tiniest nanocrystals, the hydrogen atoms are distributed in grain boundary of nanocrystal silicon grains. But by electric field application to the thin film along the surface, the smallest nanocrystals disappear and, partially, the crystal structure is destroyed. By annealing, the opposite tendency is observed. The third assumption is the creation of excited hydrogen molecule inside the silicon film by annealing to the temperatures 150–200°C: Si-H + Si-H→Si-Si + H^*_2 [8]. It is clear that the silicon nanocrystal fraction decreases but the broad spectral line for amorphous phase significantly increases. The fourth mechanism is a deep valence hole and negatively charged OH- created by laser beam irradiation [9] (**Figure 13**).

The pump-probe laser picosecond spectroscopy data with phonon-stimulated stress pulses [10] confirm the existence of the quantum interference of closed neighbor levels resulting in quantum beats phenomena (see **Figure 3**). The estimation of the energy difference of level position is around 5 μeV. Picosecond acoustic longitudinal stress pulses cause the small displacement of interface media surrounding the silicon nanocrystals because the Si-O-Si bridges were slackened and the oxygen atom oscillates between two stable excess states of four coupled pairs of silicon atoms. The main principle of switching is a motion between two silicon coupled atoms with oxygen from one pair of silicon atoms to another. R. Biswas and coworkers proposed the flip model for hydrogen incorporation in amorphous silicon with two stable opposite positions for hydrogen atoms with axial symmetry relative to the bonding silicon atom [11].
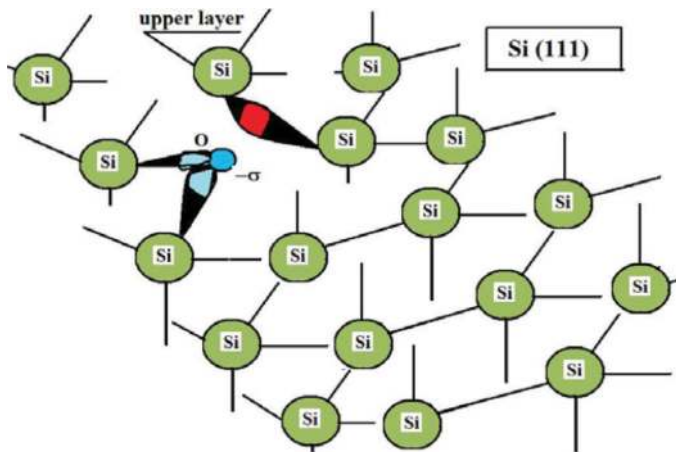

Figure 13. Scheme of AI defect location in silicon film with crystal orientation (111).

The energy of Si-O-Si bridge interaction can be written in form of Morse function

$$U = U_0\left(1 - \exp(-\alpha(x - d))\right)^2 + U_0\left(1 - \exp(-\alpha(x + d))\right)^2 \tag{6}$$

where U_0 is the energy of Si-O (4.5 eV) and α is the coefficient. The oxygen atom in A center oscillates between two points of stable positions. The change of the spatial position of oxygen atom can be described by using simple model of oscillator

$$\ddot{x} + \gamma \dot{x} + \omega_0{}^2 x = f_0 \cos\left(\Omega t\right) \tag{7}$$

where the eigenfrequency of oscillating oxygen atom can be expressed as $\omega_0 = \sqrt{\frac{1}{M}\left(\frac{d^2 U}{dx^2}\right)}$; $\gamma = \frac{kT}{h}$, k is Boltzmann constant. The solution of equation by the resonance conditions (by the $\omega_0/\gamma \gg 1$) can be written as

$$x(t) = e^{-\gamma t}\left(\frac{f_0}{2\omega_0{}^2}\sin\left(\omega_0 t\right) + \frac{f_0}{2\gamma\omega_0}\cos\left(\omega_0 t\right)\right) - \frac{f_0}{2\gamma\omega_0}\cos\left(\omega_0 t\right) \approx -\frac{f_0}{2\gamma\omega_0}\left(1 - e^{-\gamma t}\right)\cos\left(\omega_0 t\right).$$

The eigen frequency value for Si-O bond was estimated by means of the FTIR spectroscopy technique. It equals approximately to $3 * 10^{13}$ Hz. The resonance will be by the equality between the phonon frequency Ω and ω_0 value.

2.2.4. Model of vacancy with oxygen as two coupled oscillators

For the vacancy-oxygen atom (VO) defect center the model of two coupled oscillators is much more convenient:

$$\ddot{x}_1 + \gamma \dot{x}_1 + \omega_0{}^2 x_1 + ax_2 = f_0 \cos\left(\Omega t\right) \tag{8}$$

$\ddot{x}_2 + \gamma \dot{x}_2 + \omega_0{}^2 x_2 + bx_1 = f_0 \cos\left(\Omega t\right)$ and the energy of atom interaction can be expressed as the following for two pairs of silicon atoms which are oriented along the x and z axis:

$$U = U_0\left(1 - \exp(-\alpha(x_1 - d))\right)^2 + U_0\left(1 - \exp(-\alpha(x_1 + d))\right)^2 + U_0\left(1 - \exp(-\alpha(x_2 - d))\right)^2$$
$$+ U_0\left(1 - \exp(-\alpha(x_2 + d))\right)^2$$

where x_1 and x_2 are the displacement values for oxygen atom positions relatively, Si-Si$_A$ and Si-Si$_B$ pairs.

The solution of the system of two two-order differential equations contains two eigen frequencies w_1 and w_2. The oxygen atom oscillates in A center with two different frequencies corresponding two energy levels for oxygen atom. The quantum beats are observed in picosecond laser spectroscopy experiments shown on **Figure 19** caused by quantum interference of two energetic states of oxygen atom.

2.2.5. Dipole moments of Si-O bond and Si-O-Si bridge

By using the Slater atomic orbital for Si and O atoms which were written in my previous work [12] we can easily estimate dipole moment for S-O configuration. Dipole moment by the zero displacement is $\mu_{Si-O} = ex \int_V \psi_{3pSi}\psi_{2pO} dv = 4\pi ex \int_0^{2\pi} \int_0^{\xi} \int_0^{\pi} \Psi_{3p_xSi}\Psi_{2p_xO} r^2 d\phi dr d\theta$; where $dv = 4\pi r^2 dr$, $0 < r \le \xi$, ζ is covalent radius of oxygen atom, x is bond length. For 3pSi-2pO orbital bonding we can $\int_0^{\pi} \sin^2\theta d\theta = \frac{\pi}{2}$; $\int_0^{2\pi} \cos^2\phi d\phi = \pi$;

$$\mu(r) = 230ea_0 \exp\left(\frac{-3.655r}{a_0}\right)\left[0.27\left(\frac{r}{a_0}\right)^5 + 0.37\left(\frac{r}{a_0}\right)^4 + 0.41\left(\frac{r}{a_0}\right)^3 + 0.37\left(\frac{r}{a_0}\right)^2 + 0.18\left(\frac{r}{a_0}\right) + 0.05\right]$$ By
r = 1.6 Å, $r/a_0 = 3$, we can estimate the dipole moment value as $\mu_{Si-O} = 1.12$ D.

The comparison of calculated overlapping integrals as a function of distance is shown in **Figure 14**. It is seen that the Si-Si orbital is more significant even at large distances than Si-O.

For Si-O-Si bridge we can obtain

$$\mu_{Si-O-Si} = 4\pi e \int_0^{\xi} \int_0^{2\pi} \int_0^{\pi} \Psi_{3pSi'}\Psi_{3pSi''} r \Psi_{2pO'}\Psi_{2pO''} r^2 dr d\phi d\theta. \tag{9}$$

We can evaluate the dipole moment by zero displacement $\mu^0_{Si-O-Si} = 0.17D$. For Si-O-Si bridge the angle (see **Figure 15**) between two bonds is approximately $90-180°$. It is clear that by $\alpha \to 180°$ the vector value of dipole moment is zero, but by $\alpha \to 90°$ the dipole moment can be estimated as $\mu_{Si-O-Si} \approx 1.4\mu_{Si-O}$.
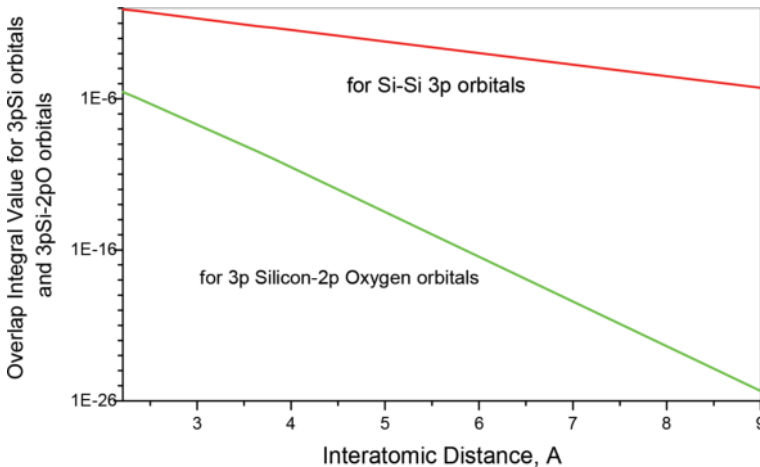

Figure 14. Overlap integrals for 3pSi-3pSi and 3pSi-2pO orbital as a function of inter atomic distance.
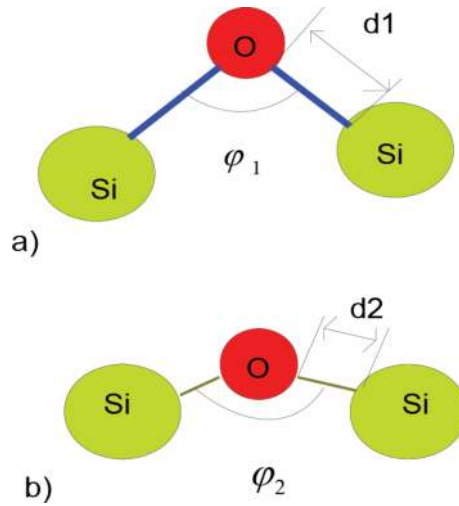
Figure 15. Si-O-Si bridge with (a) greater value of dipole moment; (b) smaller value of dipole moment, $d\varphi = \varphi_2 - \varphi_1$; $\Delta = d_1 - d_2$; d_1, d_2 are bond lengths.

By applied electrical field the dipole moment value for Si-O-Si bridge is defined by displacement evolution: $\mu = \mu^0 + \mu_x(t) \approx ex(t)$. In the case of $\mu < \mu_{critical}$ there is no localized bonded state. It is clear that for $\mu^0_{Si-O} > \mu_{critical}$ there is localized bonded state for electron, but for $\mu^0_{Si-O-Si} < \mu_{critical}$ such a state cannot exist because the Si-O bonding by zero displacement generates localized electron states on Si (111) surface which can cause troubles for writing and storing procedures of memory cell. By the annealing of Si (111) substrate to a temperature of more than 250°C we can eliminate the Si-O bonds and produce the strong siloxane bonding. Therefore, it is possible to prepare the oxidized Si (111) surface with strict siloxane Si-O-Si bridges without localized electron states on the surface. Applying the electrical or even acoustical field we can stimulate A center switching inside the film that causes the appearance of localized electron states. The polarization wave generated by laser radiation is given by

$$P = \overset{\approx}{P}(z)\exp(i(\Omega t - kz))\exp(-\gamma t) \tag{10}$$

We can estimate the yield of interference of two polarized waves with shift of phase's π.

$$\begin{aligned} P_{sum} &= P_+ + P_- = \overset{\approx}{P_{sum}}\cos(\Omega t + \phi); \overset{\approx}{P}\exp(i\phi) = \overset{\approx}{P_-}\exp(i\phi_1) + \overset{\approx}{P_+}\exp(i\phi_2); \\ \overset{\approx}{P^2} &= \overset{\approx}{P_-}{}^2 + \overset{\approx}{P_+}{}^2 + 2\overset{\approx}{P_-}\overset{\approx}{P_+}\cos(\phi_2 - \phi_1) \end{aligned} \tag{11}$$

The spatial distribution of charges for polarized molecular bridges Si-O-Si on the clean Si (111) surface is used for electrical charge trapping. The potential energy barrier for electron trapping can be estimated as

$$W \approx 2 \tilde{\tilde{P}}_+ \tilde{\tilde{P}}_- \sin \left(\phi_2 - \phi_1 \right) \Delta \tilde{\tilde{\phi}}; \ \Delta \tilde{\tilde{\phi}} = \frac{\pi \Delta d}{\lambda} \tag{12}$$

where Δd is the cell size and λ is the wavelength of polarization wave. By applied electrical field 10^7 V/m $W \approx 100$ μeV and by the value of field 10^8 V/cm is 1 meV.

Figure 16 illustrates the point defect on silicon (111) surface caused by a silicon atom vacancy and oxygen atom incorporation into the silicon network. There are three silicon bonds which are connected with oxygen atom through the sp_3 orbitals. Oxygen $2p_x$ and $2p_z$ orbital cause the splitting to the bonding and anti-bonding electron states. According to the perturbation theory the H_{11}, H_{22}, H_{33} and H_{44} are the energies for p orbitals that interacted with themselves. It is clear that such configurations are produced, and switching of interacted orbitals between them can be expressed in diagonal and non-diagonal terms of matrix of Hamiltonian:

$$\begin{pmatrix} H_{11} & V_{12} & V_{13} & V_{14} \\ V_{21} & H_{22} & V_{23} & V_{24} \\ V_{31} & V_{32} & H_{33} & 0 \\ V_{41} & V_{42} & 0 & H_{44} \end{pmatrix} \rightarrow \begin{pmatrix} H_{11} & V_{12} & V_{13} & 0 \\ V_{21} & H_{22} & V_{23} & V_{24} \\ V_{31} & V_{32} & H_{33} & V_{34} \\ 0 & V_{42} & V_{43} & H_{44} \end{pmatrix}; \tag{13}$$

2.2.5.1. Si$_3$H-$^\sigma$ vacancy defect

The molecular-like spectrum of electron states for hydrogenated cluster Si$_3$H$^{-\sigma}$ has a series of electron states in the range from 0.7 to 1.0 eV. [13]. The eigen frequencies of oscillator Si$_3$-H are conjugated with the electron states for the same oscillators and results in appearance of broadening in the electron spectra. The defect can be described as tied three Si$_3$-H oscillators and one Si$_3$- oscillator. It is clear that the quantum properties of defect are reflected in their molecular orbital spectral positions. It should be observed surely for nanostructured silicon films with structured cell less than 1 nm or for amorphous hydrogenated silicon film. In such
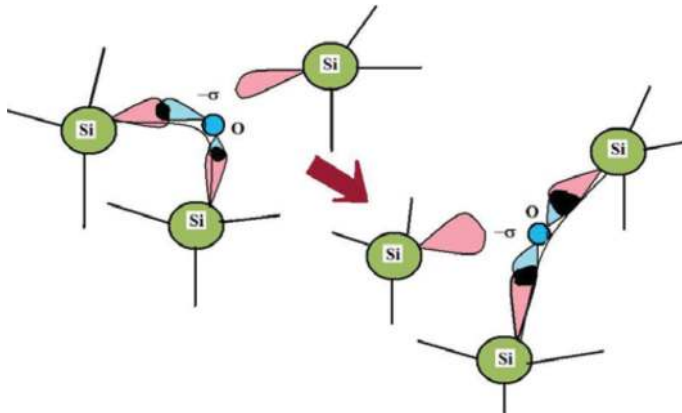

Figure 16. The point defect migration on the silicon surface (111) by applied electric field. Wave function is distributed among the 12 silicon atoms.

kind of media we surely can change the spectral positions of electron states by using bias voltage.

2.2.5.2. Si$_3$-F vacancy defect

Silicon functional groups can be determined as the following: Si-Si, Si-H, Si-H$_2$, Si-H$_3$, SiH$_2$-F. The silicon bonding is arranged according to sp^3 hybridization: *3s* spin-paired electrons and *3p* electrons. The greatest energy of bonding is for Si-F bond equal to 135 kcal/mol, but for Si-H and Si-Si, it is 76 and 53 kcal/mol, respectively. The dipole moments due to the great value of electronegativity of fluorine atom will be significant. Accordingly, the charge distribution of electron density in the SiH$_3$-F molecular group is the following: for Si atom is it is +1.1, for H atom it is −0.15, and for F atom is −0.67 [14].

2.2.5.3. Si-O$_x$ clusters

We assume that the defects are localized in Si-SiO$_2$ interface with complex composition of SiO$_x$. The oxygen atoms and dimers are incorporated in the silicon grain boundary and have weak covalent bonds with silicon. But the activation energy for molecular diffusion is low, 0.3 eV, in contrast with the activation energy value for atomic diffusion (1.3 eV). The increase in oxygen concentration results in increasing SiO bond length. For the sample with smaller grain size the hydrogen termination of dangling bonds is greater, and density of oxygen is low. But the film with large grains contains a great amount of oxygen in Si-O-Si and SiO$_2$ compositions. We assume that the exponential electron density decay is due to the exciton state decay. The short relaxation time can be described as possible relaxation process through the oxygen incorporation-related defect states, where density of states is the following: $n(E) = (n_{Si}(E) + xn_o(E))/(1 + x)$ [15].

The oxygen atom bonding with silicon atoms inside crystallites forms the dioxide composition along with defect production. **Figure 17** shows the two kinds of oxidized surfaces: Si (100) surface annealed by 1100 K and oxidized poly-Si film with a great value of <δ> = 17.6 nm. The oxide-silicon configuration for both surfaces is different. The Si (100) surface contains mainly the SiO$_2$ component with a high density of oxygen concentration but the poly-Si film is weaker oxidized with the presence of SiO$_{0.5}$ configuration.

Figure 18 illustrates the oxygen incorporation into silicon grain boundary after transformation of the silanol groups into strong siloxane bonds.

3. Field-assisted crystal phase creation from amorphous

3.1. Fractal character of restored crystal phase

The first mechanism that can be used for explanation of crystal phase restoration phenomenon in silicon film is a difference in structural orders of silicon crystal structure and polysilane chains which are arranged into conglomerates after hydrogen migration, and further incorporation is
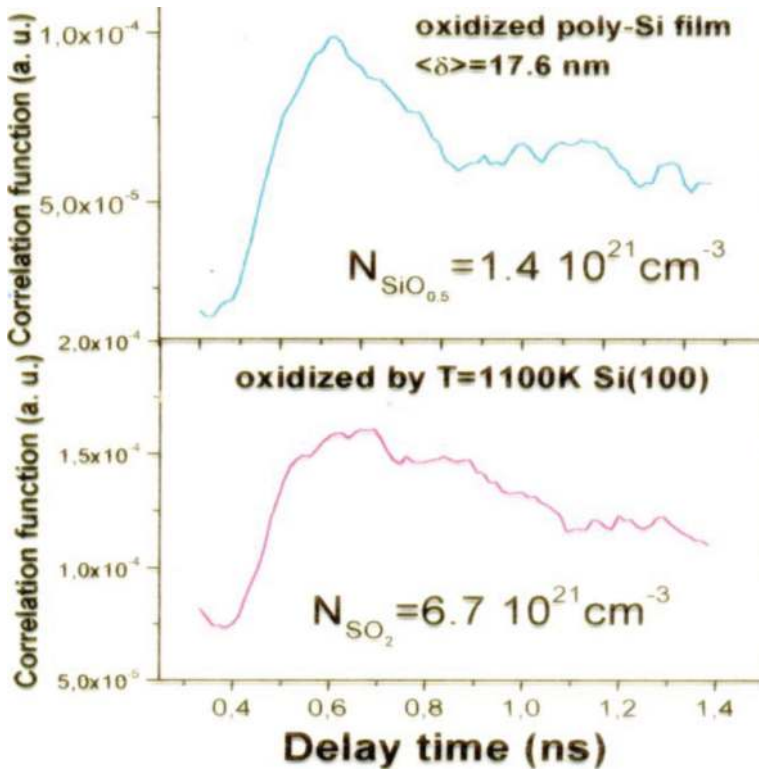
Figure 17. Correlation function g (τ) as a function of delay time between pump and probe pulses.
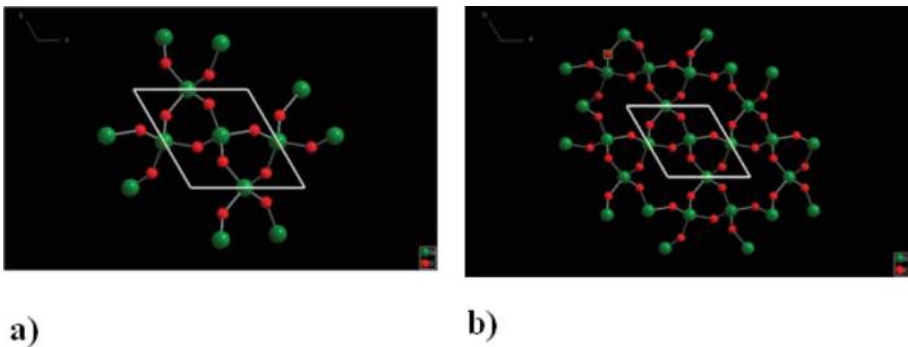

Figure 18. Silicon-oxygen incorporation in the grain boundary after transformation the silanol groups into strong siloxane bonds (a) 13 silicon atoms incorporated with 14 atoms of oxygen (SiO_x, x ≈ 1)by the Si-O bond angle equal to 130° the width of interface is 8.86 Å; (b) 29 silicon atoms incorporated with 39 oxygen atoms (x ≈ 1.34) create the intercrystal space with width equal to 14.77 Å.

transformed into the silicon net. The hydrogen surface diffusion by annealing also changes the phase fraction ratio in the silicon film. **Figure 19** shows the microphotography of silicon microcrystal that contains fractal structures of silicon bonding. By applying the external electrical field, the dipole orientations change to compensate the external field. Because the dipoles' reorientations cause numerous dislocations inside silicon nanocrystal, it is supposed that the order of crystalline structure inside the silicon film as grown usually is the same as order of fractals which is shown in **Figure 19**. The microphotography of the microcrystal of silicon on the glass substrate that is shown in **Figure 19a** demonstrates the hexagonal structure of the crystal along with fractal structures which are illustrated in **Figure 19b**. Because there is the necessity to analyze the mechanism of field-assisted phase transformation as destruction or phase restoration of native fractal nanoscale structures of silicon nanocrystals, for fractals, the dimension of Hausdorf can be surely evaluated as $d_C = -\lim \frac{\lg N(s)}{\lg(s)}$, where N(s) is the number of cubic volumes from which it is possible to substitute the rectangular nanocrystal with crystal orientation (111). Such a value of dimension equals 2.5. For determination of any structure the formula for Hausdorf metrics that is given by.

$$\rho(x.y) = \sqrt{\sum_{i=1}^{n} (x_i - y_i)^2} = 2\varepsilon$$ is suitable, where ε is radius of the open ball with centers in

points X and Y. The space limit for the fractal structure can be evaluated using the silicon bonding size 2.5 Å. For small 3D objects such as nanocrystals, the density of substitution can be written as $N_V = 1/\varepsilon^3$. For a fractal set the set capacity D_c can be written as the following: $N_V = 1/\varepsilon^{Dc}$: $D_C = \lim \frac{\log N(\varepsilon)}{\log \varepsilon^{-1}}$ by the changing of value ε by this way ε➜0.

The second proposed mechanism of silicon crystal phase restoration can be illustrated by means of **Figure 19**. It is shown that the dislocations and dipoles in grain boundary of nanocrystal under the influence of external electric field cause the phase destruction into the arc series according to the modular group scenario. Such transformations cause the appearance of numerous arcs which will be destroyed after further triangular Knop scenario of transformation of the 2D silicon structure to 1 D silicon structure or polysilane chain. For the fractal structure the Hausdorf dimension can be varied and is less than 1. The down picture on **Figure 8** illustrates the creation of Kantor dust [16] by dividing the triangular angle on the top
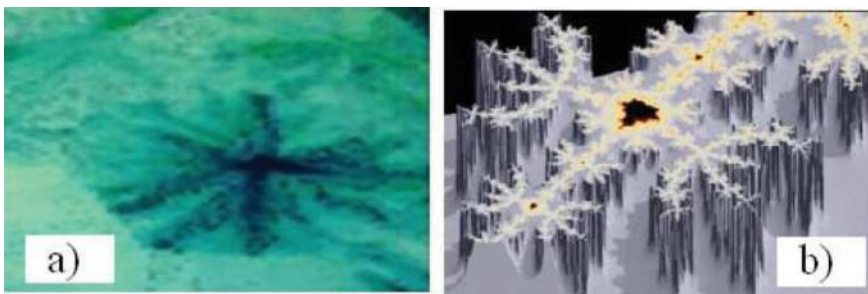

Figure 19. Photo of microscopic silicon crystal on glass substrate (a), and fractal structure of Mandelbrot set (b).

and neglecting the area of triangle in the middle of primary triangle area. For such transformation the equations for triangular quantities $X_N = 2X_{N+1}$ and for areas $S_N = 2.63^{d*}S_{N+1}$. Comparative analysis of last two equalities results in $2.63^d = 2$. The estimated value of Hausdorf dimension for such mathematical set is 0.72, because, there is a decrease in dimension by the destruction mechanism for media. It is obviously that the field-assisted transformation of silicon nanocrystals into objects with low dimension can be followed by the way of a polysilane chain creation $R_S = \frac{l\sqrt{n}}{\sqrt{6}};$.

3.2. Raman spectra of silicon film with the created crystal phase

Figure 20 illustrates the Raman spectra of amorphous silicon film which is deposited by magnetron sputtering atoms of Pt and further applying the external electric field. The scheme of experiments is shown in the figure. There is a crystal phase that was created by fixed value of applied electric field due to the charges accumulated by Pt clusters. Change in free energy by local field results in the appearance of silicon stripes of the crystalline phase in amorphous silicon.

Free energy functional can be expressed as follows

$F_{FE} = \int_V \left(\frac{1}{2}\varphi \left[\left(q_0^2 + \nabla^2\right)^2 + a \right]\varphi + \frac{1}{4}\varphi^4 \right) dV$, where q_0 is a phenomenological parameter and φ is a dimensionless average density. The solution of equation is

$$dF_{FE} = \frac{\partial F_{FE}}{\partial \varphi}\frac{\partial \varphi}{\partial t}dt + \frac{\partial F_{FE}}{\partial \varphi}\frac{\partial \varphi}{\partial x}dx + \frac{\partial F_{FE}}{\partial \varphi}\frac{\partial \varphi}{\partial y}dy + \frac{\partial F_{FE}}{\partial \varphi}\frac{\partial \varphi}{\partial z}dz = 0 \qquad (14)$$
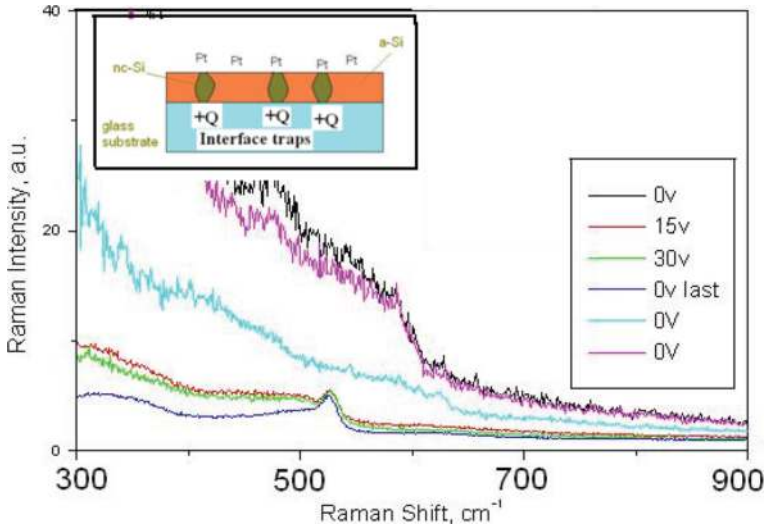

Figure 20. Raman spectra of amorphous silicon film deposited by magnetron sputtering atoms of Pt and further applying the external electric field.
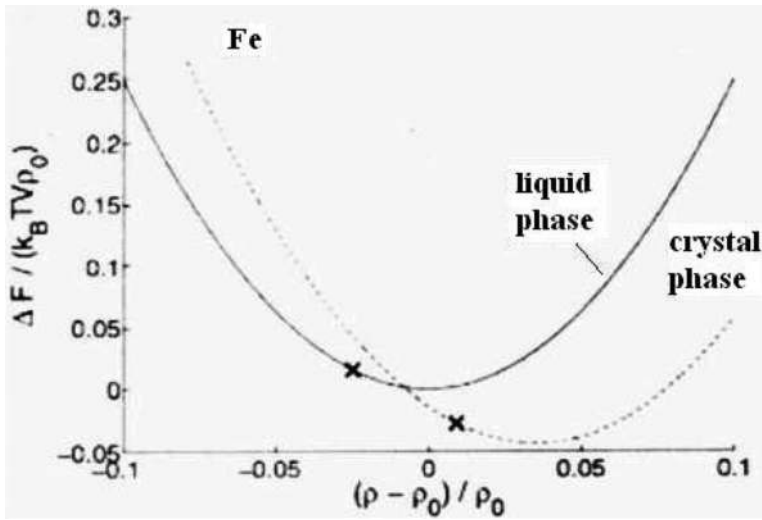
Figure 21. Free energy as a function of reduced particles density at the melting point of Fe according to the phase-field crystal model estimations [17].

or finding the minimum of the functional results in the investigations of crystal phase creation. For 1D in the uniform phase the expression $\psi(x^-) = \sum_j A_j(t)\exp\left(ik_j^{\rightarrow x\rightarrow}\right) + \psi^-$ can be used as a possible solution. **Figure 21** shows free energy as a function of reduced particle density at the melting point of Fe according to the phase-field crystal model estimations.

3.3. Renormalization group of translation for crystal phase creation

The resolving the equations for locality function by the free energy functional minimizing [17]:

$\frac{\partial\psi}{\partial t} = \nabla^2 \frac{\delta F_i}{\delta\psi} + \eta$; for ψ locally conserved, and $\frac{\partial\psi}{\partial t} = -\frac{\delta F_i}{\delta\psi} + \eta$; for ψ locally non-conserved, from which we can easily find the equation for estimating the value of energy for order–disorder transition:

$\nabla^2 \frac{\delta F_i}{\delta\psi} + \frac{\delta F_i}{\delta\psi} = 0$; also, it is assumed that the evaluation value of free energy (of heat) equals the energy of local field force to arrange in order all the atoms which should be placed on their sites: $\delta F \approx \mu E_{Local} - T\delta S$.

The solution of nonlinear Swift-Hohenberg equation also can be presented as a linear combination of solutions if we derive the terms of ψ as partial solutions and further combine them. The ψ local function can be transformed into a series according to perturbation theory as follows $\psi = \psi_0 + \varepsilon\psi_1 + \varepsilon^2\psi_2 + \varepsilon^3\psi_3 + \varepsilon^4\psi_4 + ...$, where the value ψ_0 is a steady-state solution, and next values are the next order of perturbed decomposing procedure. For such a purpose it can be used as a first order of the solution that can be expressed as: $\psi_1 = P_1(x,t)\exp(ik) + Q_1(x,t)\exp(2ik) + R_1(x,t)\exp(3ik) + c.c.$ and amplitude $A_j(t) = A_j(X,t)$ $\left(1 + \sum_{j=1} \varepsilon^j Z_j\right)$, where Z_j is a renormalization constant [18].

Author details

Dmitry E. Milovzorov

Address all correspondence to: dmilovzorov2002@yahoo.com

Fluens Technology Group Ltd., Moscow, Russia

References

[1] Tsu R, Gonzalez-Hernandez J, Chao SS, Lee SC, Tanaka K. Critical volume fraction of crystallinity for conductivity percolation in phosphorus-doped Si: F: H alloys. Applied Physics Letters. 1982;**40**:534. ISSN: 0003-6951

[2] Lucovsky G, Nemanich RJ, Knight JC. Structural interpretation of the vibration spectra of a-Si:H alloys. Physical Review B. 1979;**19**:2064-2073. ISSN: 0163-1829

[3] Yu P, Cardona M. Fundamentals of Semiconductors. Berlin: Springer; 1996. p. 617. ISBN: 3-540-61461-3

[4] Kahan VD. High frequency hopping transport in solids and dielectric transparency in compensated semiconductors. JETP. 2000;**117**:452-456. ISSN: 1063-7761

[5] Powell MJ, Deane SC. Improved defect-pool model for charged defects in amorphous silicon. Physical Review B. 1993;**48**:10815-10826. ISSN: 0163–1829

[6] Watkins G, Corbet JW. Defects in irradiated silicon I: Electron spin resonance of the Si-A center. Physical Review. 1961;**121**:1001-1014. ISSN: 0163-1829

[7] Watkins G, Corbett JW. Physics Review. 1965;**138**:A543. ISSN: 0163-1829

[8] Jones B, Coomer BJ, Goss JP, Hourahine B, Recende A. The interaction of hydrogen with deep level defects in silicon. Solid State Phenomena. 1999;**71**:173-248

[9] Bakos T. Defects in amorphous SiO2: reactions, dynamics and optical properties [PhD Thesis]. Nashville; 2003. p.70

[10] Milovzorov D. Electronic structure of nanocrystalline silicon and oxidized silicon surfaces. Electrochemical and Solid State Letters. 2001;**4**(7):G61-G63. ISSN: 0013-4651

[11] Biswas R, Li Q, Pan BC, Yoon Y. Mechanism for hydrogen diffusion in amorphous silicon. Physical Review B. 1998;**57**:2253-2256. ISSN: 0163-1829

[12] Milovzorov D. Memory cell with photoacoustic switching. In: Lai WY, Pau S, Daniel Lopez O, editors. Proceedings of the SPIE 5592. Nanofabrication: Technologies, Devices, and Applications. 2005. pp. 427–437. DOI: 10.1117/12.568290

[13] Xu C, Taylor T, Burton G, Neumark D. The Journal of Chemical Physics. 1998;**108**:7645. ISSN: 0021-9606

[14] Voronkov M. Topics in Current Chemistry. 1986;**131**:99. ISSN: 0340-1022

[15] Lanoo M, Allan G. A cluster plus effective tight-binding study of SiO_x systems. Solid State Communications. 1978;**28**:733-739. ISSN: 0038-1098

[16] Hausdorff F. Grundzuge der Mengenlehre. Vol. 184. Berlin; 1914. ISBN: 3-540-42224-2

[17] Athreya B, Goldenfeld N, Dantzig J. Renormalization-group theory for the phase-field crystal equation. Physical Review E. 2006;**74**:011601. ISSN: 0163-1829

[18] Emmerich H, Granasy L, Lowen H. Selected issued of phase-field crystal simulations. The European Physics Journal Plus. 2011;**126**:102. ISSN: 2190-5444